Transport of ions during ion implantation

G. J. Parker,[1] W. N. G. Hitchon,[2] and E. R. Keiter[2]
[1]*Lawrence Livermore National Laboratory, 7000 East Avenue, L-418, Livermore, California 94550*
[2]*Materials Science Program and Engineering Research Center for Plasma-Aided Manufacturing, University of Wisconsin-Madison, Madison, Wisconsin 53706-1691*
(Received 19 May 1995; revised manuscript received 26 February 1996)

An efficient scheme for the description of long-mean-free-path particle transport at a kinetic level has been extended to a case where particle distributions are highly anisotropic: implantation of ions into a solid. The method calculates the scattering rate of particles throughout a region and obtains the particle distribution from the scattering rate. The scattering rate is found by using a numerical form of a propagator to solve an integral equation. The propagator is the probability that a particle that scattered in a cell has its next scatter in any other cell of the mesh. The main focus of this work is the way this propagator can be computed efficiently and accurately for an arbitrary angular distribution of scattered particles as compared to other computer models. The method is illustrated in application to implantation of dopants into silicon. [S1063-651X(96)08507-8]

PACS number(s): 02.70.−c, 05.20.Dd, 68.55.Ln

I. INTRODUCTION

In this paper we describe an efficient, nonstatistical numerical technique for calculation of particle distribution functions. The method is applicable for an arbitrarily varying mean free path in situations where individual particle motion between collisions does not involve nonlinear interactions between the particles themselves. The present work extends an earlier method to the case where the particle distribution function is highly anisotropic. The method used here to find the depth profile of the implanted ions from the ion distribution at the surface is referred to as a ''transition-matrix'' (TM) technique. The techniques presented allow detailed, spatially resolved predictions of the dopant profile to be obtained, efficiently enough to be used to optimize the implantation system design.

The implantation of energetic ions into a solid has in the past been described by Monte Carlo [1–3] or Fokker-Planck–Boltzmann [4,5] calculations of the ion trajectories in the solid. In this paper we employ a nonstatistical transition-matrix [6–8] description of the ion motion that is much more efficient than Monte Carlo methods in multiple dimensions where statistical fluctuations in peripheral areas (i.e., low-dopant-concentration regions) can be a severe problem [3]. While the TM method can be considered an extension to conventional Fokker-Planck–Boltzmann methods, it is more accurate in multiple dimensions. The method involves numerically solving an integral equation for the scattering rate of particles and for the angular distribution of scattered particles. The key to the method is to be able to set up a numerical ''propagator'' (or kernel), which we call the transition-matrix, which is compact, accurate, and can be used efficiently. The input to the calculation in the solid is the ion velocity distribution at all points along the surface.

The TM description of the ion motion in the solid is outlined in Sec. II. In Sec. III we describe the setting up of the TM in more detail. The results of calculations are then given in Sec. IV for a set of implantation conditions, where calculated doping profiles and spatial distributions are presented.

II. TRANSITION-MATRIX DESCRIPTION OF PARTICLE MOTION

In this section we describe the numerical scheme used in this work. The procedure is fully kinetic and is equivalent to solving the Boltzmann equation in terms of the information it provides. However, instead of calculating the distribution function directly as in Ref. [4], we find in each phase-space cell the scattering rate or, more precisely, the distribution of particles that scattered in that cell of the numerical mesh. The total distribution in the cell consists of particles that scattered there and particles passing through the cell that scattered elsewhere. Once the distribution of scattered particles is known, the total distribution can easily be found from it. There are two advantages to finding the distribution of scattered particles first.

(i) The scheme updates the distribution iteratively by calculating successive scattering rates in all the cells of the mesh. (The procedure described in this version of the TM method does not follow the time dependence in detail, therefore.) Each iteration takes the distribution of scattered particles from each cell and advances it to the next cells where scattering occurs, for all the particles. The procedure employs very large steps since each ''step'' corresponds to the motion between successive collisions. This is very efficient and reduces the numerical diffusion by minimizing the number of times the particle scattering rate is replaced on the mesh.

(ii) If (as is often the case) the angular distribution of scattered particles in each cell can be stored using a simpler representation than can the full distribution function of all the particles in the cell, the storage requirements are reduced by a very large factor.

In this TM method we calculate the number of particles scattering and their angular distribution in each phase space cell of the mesh. The phase space considered here includes the three spatial dimensions and the kinetic energy of the ion as a fourth variable. We first describe the physical processes of ion implantation and then how the TM describes it numerically.

The physical process of ion implantation can be under-

stood as a series of individual events. First an ion travels some distance in space (which we call a ''ballistic'' movement) before undergoing a nuclear collision with an atom in the solid. Both the direction and the distance the ion travels depend on the initial velocity. On average the ion will travel a mean free path λ, which depends on its initial velocity. Once the ion suffers a nuclear collision, its velocity changes in both direction and magnitude. Eventually, after numerous ''generations'' of ballistic moves followed by nuclear collisions, the ion's kinetic energy is lost and the ion comes to rest somewhere inside the solid.

In the TM method the above physical picture is implemented on a numerical mesh. The first part of this mesh is a Cartesian mesh in three dimensions, which divides the solid into small volumes. Each volume cell, denoted by c', contains another mesh. This mesh is a discretization of the ion's kinetic energy E'. Each cell of this mesh has an average energy E' and width dE' associated with it. For each spatial cell c' and for each E' the scattering rate of ions is computed. Furthermore, an average velocity $\vec{V}^{dr}(c',E')$ of the ions is also computed (see below).

We will now outline how the scattering rates $R(c',E')$ are iterated on the mesh. Let us consider a spatial cell c' and a group of ions at energy E'. This group of ions scatters at a rate $R(c',E')$ and has an angular distribution $f(\theta,\phi,c',E')$. $f(\theta,\phi,c',E')$ is the probability that an ion with energy E' that last scattered in cell c' is moving in a direction within the range ϕ to $\phi+\Delta\phi$ and θ to $\theta+\Delta\theta$ (the method used to compute f is described in Sec. III A). $\theta=0$ is along the Cartesian z axis (which is defined to be normal to the target surface) and ϕ is measured from the Cartesian x axis.

For given $f(\theta,\phi,c',E')$ we need to know the probability that an ion will next scatter in cell c. The ballistic TM $T_{\rm bal}(c;c',E',f)$ is exactly this probability. The rate of ions with energy E' scattering in cell c having come from c' is $T_{\rm bal}(c;c',E',f)R(c',E')$. The total scattering rate in cell c is the sum over all spatial cells

$$R(c,E')=\sum_{c'} T_{\rm bal}(c;c',E',f)R(c',E'). \tag{1}$$

One important feature of the way we construct the ballistic TM, which is explained in Sec. III C, is that we only need to store a three-dimensional array to obtain $T_{\rm bal}$.

The use of Eq. (1) is illustrated in Fig. 1. The scattering rate in the cell c can be thought of as being produced by particles scattering in all the cells c', some of which subsequently scatter in c. For example, suppose a certain cell c' has a scattering rate of $R(c',E')$ and 1% of these particles have their next scatter in cell c (i.e., the probability of the next scatter being in c is 0.01). Then the contribution of the scattering in c' to the scattering in c is given by 0.01 $R(c',E')$. When the contributions from all cells c' are combined, as in Eq. (1), we get the total scattering rate in cell c.

Once the new scattering rates $R(c,E')$ are found for each spatial cell, the ion energies are adjusted due to nuclear collisions. Another TM, the ''collision'' transition matrix $T_{\rm col}(E,E')$, is the probability that an ion with energy $E'\pm dE'/2$ will have a final energy $E\pm dE/2$ after a nuclear collision. We then have an expression for the scattering rate after allowance for nuclear collisions:

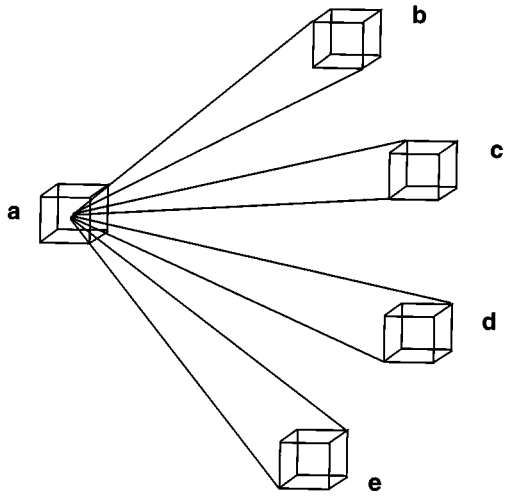

FIG. 1. Schematic showing the redistribution of particles suffering a scatter then traveling from cell a to cells $b-e$.

$$R(c,E)=\sum_{E'} T_{\rm col}(E,E')R(c,E') \tag{2}$$

for all spatial cells c.

In earlier work [6–8] we defined R to be a scattering rate per second. In this work R is the number scattering at each generation, so at, say, the third iteration of Eqs. (1) and (2) we find the total number of scatters at the third generation of scatters in a certain cell.

In this section we described the physical process of ion implantation and how the TM method calculates scattering rates. In the next section we will describe how the TMs are generated and incorporate another physical process (electronic stopping) into the TM method.

III. GENERATION OF TRANSITION MATRICES

In this section we first describe how the the angular distribution f of ions is calculated and how the TMs are generated. Detailed descriptions for nuclear collisions, ballistic motion, and electronic drag TMs are given. We finish this section with a schematic of the TM algorithm. We stress that the physical model presented here is a simplified approximation. More complicated kernels for each of the propagators could be used. However, the main purpose of this paper is to illustrate the method. Accordingly, such extensions will be incorporated at a later time.

A. Calculation of the angular distribution

The problem of finding the angular distribution of a group of ions that have the same energy in a spatial cell c can be thought of as being in two parts. First we recognize that all of the ions which scatter in the cell carry with them some velocity. During the nuclear collision, each ion is scattered, on average, through some angle $\Theta(E,E')$, which depends on the initial and final energies. We can calculate the average velocity $\vec{V}^{dr}(c',E')$ carried in by particles that scatter in the cell c from all other cells with ions at energy E' using

$$\vec{V}^{dr}(c,E') = \frac{\Sigma_{c'} T_{\rm bal}(c,c',E',f) R(c',E') [\hat{\vec{x}}\cos\phi\sin\theta + \hat{\vec{y}}\sin\phi\sin\theta + \hat{\vec{x}}\cos\theta] \sqrt{\frac{2E'}{M_1}}}{R(c,E')}, \tag{3}$$

where M_1 is the mass of the ion and (ϕ,θ) are the spherical angles subtended by a line from cell c' to c. Once in cell c, the ions suffer a nuclear collision. $T_{\rm col}(E,E')$ gives the probability of the final energy after the collision being $E \pm dE/2$. For each final energy, an average cosine of the angle scattered through can be found; the angle being $\Theta(E,E')$ (see below). By a simple average over the ensemble, one finds

$$\vec{V}^{dr}(c,E) = \frac{\Sigma_{E'} T_{\rm col}(E,E') R(c,E') \cos[\Theta(E,E')] \vec{V}^{dr}(c,E') \sqrt{\frac{E}{E'}}}{R(c,E)}. \tag{4}$$

From $\vec{V}^{dr}(c,E)$ we can construct $f(\phi,\theta,c,E)$. However, we first construct the angular distribution in another set of coordinates $g(\tilde{\theta},c,E)$, where $\tilde{\theta}=0$ points in the direction of $\vec{V}^{dr}(c,E)$. We choose the functional form of $g(\tilde{\theta},c,E)$ to be

$$g(\tilde{\theta},c,E) = \frac{1}{2}\left[1 + \frac{3|\vec{V}^{dr}|}{\sqrt{2E/M_1}}\cos\tilde{\theta}\right] \tag{5}$$

for $0 \leq \tilde{\theta} \leq \pi$ if $|3\vec{V}^{dr}(c,E)| < \sqrt{2E/M_1}$, otherwise

$$g(\tilde{\theta},c,E) = \frac{2}{(1-\cos\tilde{\theta}_l)^2}[\cos\tilde{\theta} - \cos\tilde{\theta}_l] \tag{6}$$

for $0 \leq \tilde{\theta} \leq \tilde{\theta}_l = \arccos[3|\vec{V}^{dr}|/\sqrt{2E/M_1} - 2]$ and zero otherwise. The above forms conserve probability and give the correct velocity $\vec{V}^{dr}(c,E)$. Once g is found, simple coordinate rotations to obtain $f(\phi,\theta,c,E)$ can be done [where θ $(\phi)=0$ is along the Cartesian z (x) axis].

B. Transition matrix for nuclear collisions

We now describe the physical model used in the construction of the transition matrices. We start with the straightforward collision matrix $T_{\rm coll}$. We stress that the physical models used to construct the TMs in this and the next two subsections are somewhat arbitrary and can easily be changed to a more sophisticated physical description. The purpose is to illuminate the procedure of the TM approach, not necessarily the physical model used.

We choose a model described by Lindhard *et al.* [9] and Firsov [10], where the nuclear scattering cross section may be written using the approximate one-parameter expression. They first define reduced energy and length parameters

$$\varepsilon = \varepsilon_1 E = \left(\frac{M_2}{M_1+M_2}\frac{a}{Z_1 Z_2 e^2}\right)E, \tag{7}$$

$$\rho = \rho_1 x = [N\pi a^2 \gamma]x, \tag{8}$$

where E is the initial ion energy, M_2 is the target mass, Z_1 (Z_2) is the ion (target) atomic number, e is the electron charge, N is the number density of the target, $\gamma = 4M_1M_2/(M_1+M_2)^2$, a is the screening radius

$$a = 0.8853 a_0 (Z_1^{2/3} + Z_2^{2/3})^{-1/2}, \tag{9}$$

and a_0 is the Bohr radius. They introduce the parameter

$$t = \frac{T}{\gamma E}\varepsilon^2, \tag{10}$$

where T is the energy transferred from the ion to the target. The nuclear scattering cross section may then be written using the approximate, one-parameter version

$$N d\sigma(T) = \frac{\rho_1}{\gamma}\frac{dt}{2t^{3/2}} h(t^{1/2}), \tag{11}$$

where the function h is of the form

$$h(t^{1/2}) = \lambda_0 t^{1/2-m}[1 + (2\lambda_0 t^{1-m})^1]^{-1/q}, \tag{12}$$

with $\lambda_0 = 2.54$, $m = 0.25$, and $q = 0.475$ [4] in the simulations reported here.

For each group of ions with energy $E' \pm dE'/2$, we need the probability of a final energy after the atomic scatter: $T_{\rm col}(E,E')$. The probability of an ion with initial energy E' scattering to a range of final energy $E \pm dE/2$ is proportional to the cross section

$$T_{\rm col}(E,E') \propto \int_{T_0}^{T_1} d\sigma(T), \tag{13}$$

where $T_{0,1} = E' - (E \pm dE/2)$.

Unfortunately, as T_0 approaches zero, $T_{\rm col}$ goes to infinity. This represents very-small-angle scattering. A lower limit $T_0^{\rm min}$ is imposed to avoid this problem. Since the energy transferred is related to the scattering angle Θ by

$$T = \gamma E' \sin^2(\Theta/2), \tag{14}$$

this is equivalent to resolving nuclear scattering angles above a certain limit. Since the algorithm described here has a fixed angular resolution, a typical angular cell width is used in the above equation to find the minimum energy transferred. Typical angular widths give $T/E' \sim 2\%$.

For each initial energy E', Eq. (13) is integrated over each valid final energy cell $E \pm dE/2$ to find each component

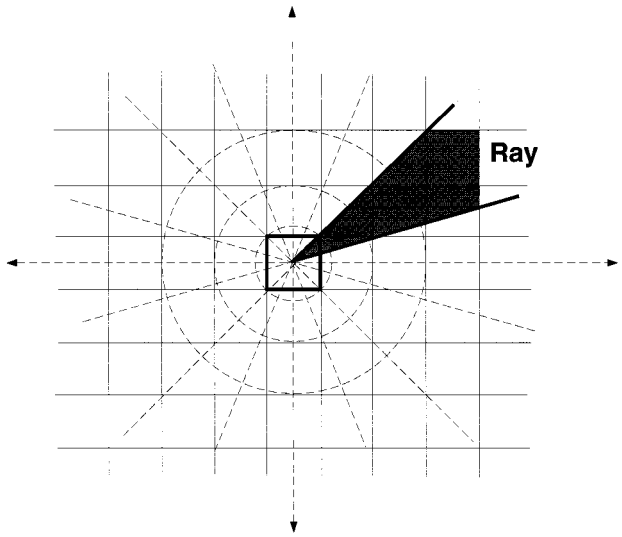

FIG. 2. Two-dimensional schematic showing ''final'' Cartesian cells overlapped by the ''beam'' from a particular initial point. Since the initial cell is not a point, the beam comes from a source of finite extent so the overlap of the beam with any Cartesian cell is obtained by integrating over all points in the initial cell. E is the final kinetic energy remaining at that radius after having undergone losses due to electronic stopping and small-angle nuclear scattering.

of $T_{\rm col}(E,E')$. The ''total'' cross section for large-angle nuclear scattering at energy E' is then

$$\Sigma(E')\equiv\int_{T_0^{\min}}^{\gamma E'} d\sigma(T). \tag{15}$$

The constant of proportionality for $T_{\rm col}$ is then simply $1/\Sigma(E')$. The small-angle nuclear scattering that we have neglected is accounted for as a viscous drag which does not change the ions direction, only their speed (see below).

C. Transition matrix for the ballistic move

We now describe the ballistic propagator $T_{\rm bal}(c,c',E',f)$, which is the probability of an ion's next scatter being in cell c, given it last scattered in cell $E'\pm dE'$ and has an angular distribution f in c'. $T_{\rm bal}$ depends not only on the spatial cells but on the energy of the ions (through the mean free path λ) and the angular distribution in cell c'. However, we do not need to construct $T_{\rm bal}$ explicitly, as we shall see.

First, $f(\phi,\theta,c',E')$ gives the probability that ions with energy E' in cell c' are moving in a beam bounded by the spherical angles ϕ to $\phi+d\phi$ and θ to $\theta+d\theta$. Once we know the number in the beam, we can take that number and distribute it among the Cartesian cells overlapped by the beam (Figs. 2 and 3).

The energy dependence of $T_{\rm bal}$ stems from the mean free path $\lambda(E')$. For each beam corresponding to a range of (ϕ,θ), we store a list of Cartesian cells whose volumes overlap with the beam. This list treats c' as being at the origin. The lth member of the list is at $(x(l),y(l),z(l))$ relative to the position of c'. The number of ions placed in each of these Cartesian cells is the number left in the beam multiplied by $h(l,\phi,\theta,E')$, the fraction of which scatter, given by

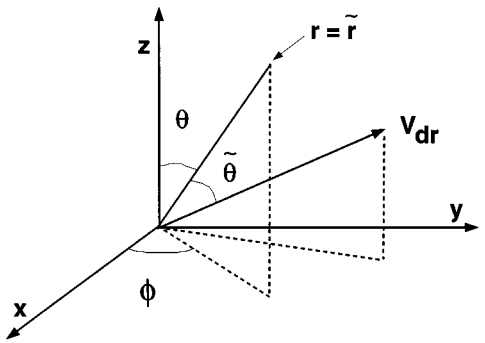

FIG. 3. Relationship between the spherical and Cartesian coordinate systems used to set up the transition matrix.

$$h(l,\phi,\theta,E')=\frac{\Delta A dr}{\lambda(E')\Delta\Omega r^2}, \tag{16}$$

where ΔA is the cross-sectional area of the part of the Cartesian cell c that is inside the beam starting at c' defined by ϕ to $\phi+d\phi$ and θ to $\theta+d\theta$. ΔA is perpendicular to that beam at constant r. The dependence of ΔA and h on c and c' is only through the differences in their Cartesian coordinates. dr is the mean distance traveled down the beam in crossing the Cartesian cell, r is the total distance traveled from the initial cell c', λ is the mean free path for the energy E', and $\Delta\Omega$ is the solid angle of the beam, defined by $\Delta\Omega\equiv\sin\theta d\theta d\phi$. Although Eq. (16) gives a good estimate if dr is small compared to λ, a better estimate is

$$1-\exp\left(\frac{-\Delta A dr}{\lambda(E')\Delta\Omega r^2}\right). \tag{17}$$

The quantity $a(l,\phi,\theta)\equiv\Delta A dr/\Delta\Omega r^2$ is an average over the Cartesian cell and is obtained by dividing the beam and the Cartesian cells into subbeams and subcells and summing over these. This quantity can be stored and later divided by $\lambda(E')$. The last part of $T_{\rm bal}$ involves computing $\lambda(E)$. $\lambda(E')$ is given by

$$\lambda(E')=\frac{1}{N\Sigma(E')}, \tag{18}$$

where $\Sigma(E')$ was computed in constructing $T_{\rm col}$ and is given by Eq. (15).

In summary, the set of quantities $a(l,\phi,\theta)\equiv\Delta A dr/\Delta\Omega r^2$ are all we need to store to find $T_{\rm bal}$. They can be computed once and stored for a given spatial and angular mesh. Even in three-dimensional space, this geometrical part of $T_{\rm bal}$ can be stored compactly and can be used for a variable λ. This approach constrains us to think in terms of traveling along beams outward from the initial cell. We first decide on which ''beam'' to follow and then we travel out along it. This restriction is acceptable since it allows $T_{\rm bal}$ to be stored compactly.

D. Electronic stopping and small-angle nuclear scattering

Large-angle nuclear scattering is not the only way for an ion to lose its kinetic energy. In addition, as the ion travels through the target, the electron gas can produce a viscous

drag. We now describe how this TM, T_{ele}, is constructed. We then describe how small-angle nuclear scattering (which can also be thought of as a viscous drag) is included with this TM.

We start with expressions similar to those of Lindhard *et al.* [9] and Firsov [10]. The expressions used to calculate the energy loss due to electronic stopping of ions are

$$dE_e = dLNS_e \tag{19}$$

and

$$S_e(E) = S_L = kE^q, \tag{20}$$

where dL is the path length, S_e is called the stopping power, $q = 1/2$, and k is given by

$$k = \frac{1.212 Z_1^{7/6} Z_2}{(Z_1^{2/3} + Z_2^{2/3})^{3/2} M_1^{1/2}}. \tag{21}$$

The expression can be integrated to give the change of energy ΔE given that the ion traveled a distance L.

$T_{ele}(c,c',E,E')$ gives the probability that, due to electron drag, the ion will drop down to a ''final'' energy E in each cell c it crosses given that it last scattered in cell c', with energy E'. Since we know the initial and ''final'' Cartesian cells, we know the average length traveled l and therefore we can find the ''final'' energy. By tabulating this we can use it to find E and $\lambda(E)$ at all points along the ion's trajectory, for use with the ballistic transition matrix.

As described previously, small-angle nuclear scattering can also be considered to be simply a viscous drag term. The energy loss due to traveling a short distance dl is given by

$$dE = Ndl \int_0^{T_0^{\min}} T d\sigma(T). \tag{22}$$

For each beam described in T_{bal}, the above equation is numerically integrated from each initial cell to each final Cartesian cell. We note that as the integration is carried out along the trajectory, the energy of the ion is changing not only due to small-angle nuclear scattering but also due to electronic drag. These energy losses change the lower bound of the integral. It is important to include this effect while one is computing the energy loss due to small-angle nuclear scattering. The corresponding energy loss is added to that which is already included in T_{ele}.

E. Algorithmic flow of the TM approach

In the previous subsections we have described each TM and the way each is constructed. We will now briefly outline the algorithmic flow of the method.

Figure 4 gives the simulation flow chart. The code first reads in the user defined input parameters, which define the spatial and energy regions of interest. The program then checks to see if the corresponding TM T_{bal} has been computed already for this set of input data. If not, control is passed to a separate module that calculates the appropriate T_{bal} and stores it permanently. Once T_{bal} is found or calculated, the other TMs (T_{coll} and T_{ele}) are computed according to the spatial and energy meshes. While these TMs could also be stored, there is not a large computational overhead in calculating them in the beginning of the simulation.

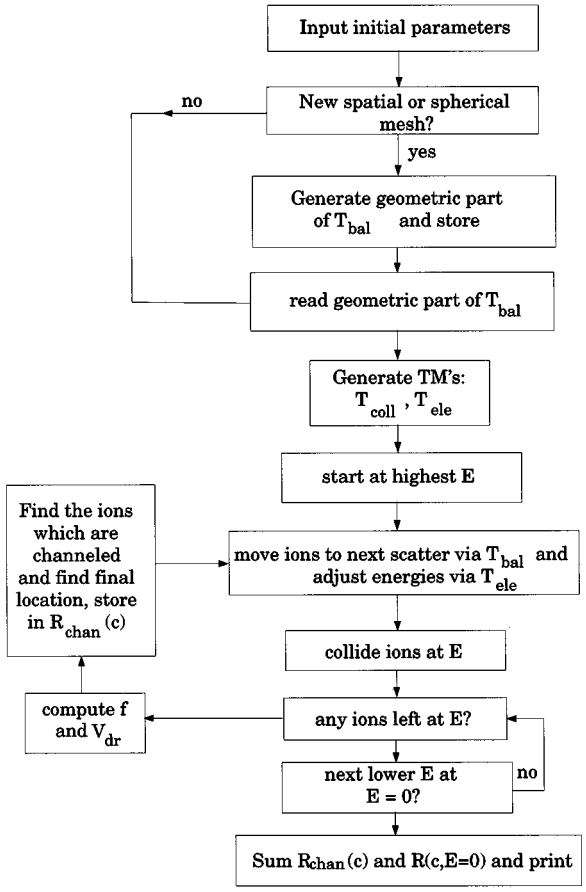

FIG. 4. Flow chart illustrating the logic flow of the transition-matrix method.

The initial ''pulse'' of ions is allowed to enter the simulation region, typically in a well-defined direction and energy. The TM T_{bal}, in conjunction with T_{ele}, is used to find the next cell in which the ion will have a large-angle scatter. The TM T_{col} then describes, for each spatial and energy cell, the distribution to final energy cells. In each spatial cell in which there are ions, if there are ions in the initial energy cell, the angular distribution f is computed and the process is iterated again starting with the TM T_{bal}. Otherwise the next lower energy cell is iterated. Eventually, the last energy cell will be emptied and the spatial distribution of the ions is found from the density in the zero energy cell at all spatial locations.

IV. RESULTS AND DISCUSSION

In this section we present results obtained from the TM method. We have simulated a boron-ion beam incident onto a silicon target. In all the simulations, the beam is tilted 7° from the z axis (which is defined to be the normal to the surface of the target) and in the xz plane. The beam strikes the surface at $x = y = z = 0$. The spatial mesh consists of 41 cells in z, 15 cells in both x and y, 20 cells in each spherical angle θ and ϕ, and 100 energy cells. The number of cells was varied and this set was found to be both accurate and efficient.

Figure 5 compares the TM results to experimental results (as given in Ref. [4]) for a 100-keV boron-ion beam injected

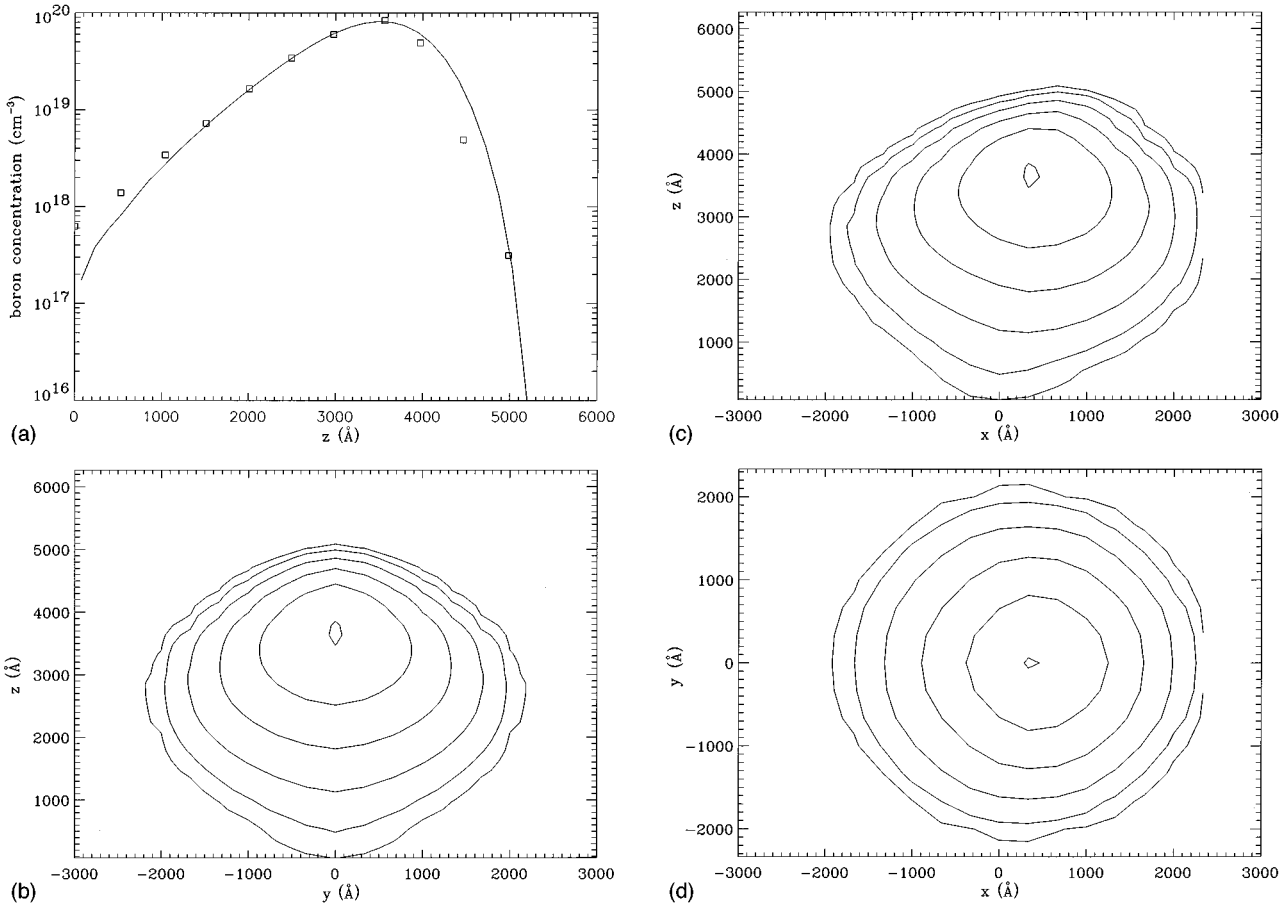

FIG. 5. Boron-ion concentration for a 100-keV injected beam into amorphous silicon. (a) Boron-ion concentration as a function of z: squares, experiment; line, TM. (b)–(d) Contour plots of the boron-ion concentration as a function of two spatial variables with the third being integrated (summed) over. Contours are 0.003 16, 0.01, 0.0316, 0.1, 0.316, and 0.95 of the maximum value.

into amorphous silicon. Figure 5(a) is obtained by summing over x and y to obtain a depth profile of the boron-ion concentration. Both experimental and TM results are shown and exhibit good agreement. Figures 5(b)–5(d) are contour plots of the boron-ion concentration as a function of two spatial variables, the third being summed over. In Figs. 5(c) and 5(d), the peak in the ion concentration is not centered at the x origin due to the small but nonzero incident angle of the beam.

As the boron ions enter the silicon, the mean free path is quite large so few ions suffer large energy losses initially. As the ions move farther in, electronic drag and small-angle nuclear scattering slow the ions until the mean free path decreases dramatically. Once this happens, the vast majority of the ions suffer large-angle nuclear scatters (Fig. 5) and come to rest near the peak of the depth profile.

Next, we vary the mass of injected ions. Figures 6 and 7 compare the computed and experimental depth profiles for injected 160-keV phosphorus and 355-keV arsenic, respectively. For the heavy ion arsenic, experimental results [11] for electronic stopping suggest that Eq. (21) is inaccurate by a factor of nearly 2. Accordingly, the stopping coefficient in Eq. (21) was multiplied by an estimated correction of 0.6 in this case. Again, we see good agreement between the TM and experimental results.

Finally, a 85-keV boron-ion beam is injected into a crystalline silicon target. In this case, the z axis (normal of the silicon surface) is also along the crystalline $\langle 111 \rangle$ axis. We have included 13 planar and 26 axial channels for this calculation. We have used the procedure described by Gibbons and co-workers [4] for the critical angles, planar widths, and final ion distribution in the channel. We do stress, as in Ref. [4], that when channeling is incorporated, it is important to allow only ions that suffer large-angle nuclear scattering to

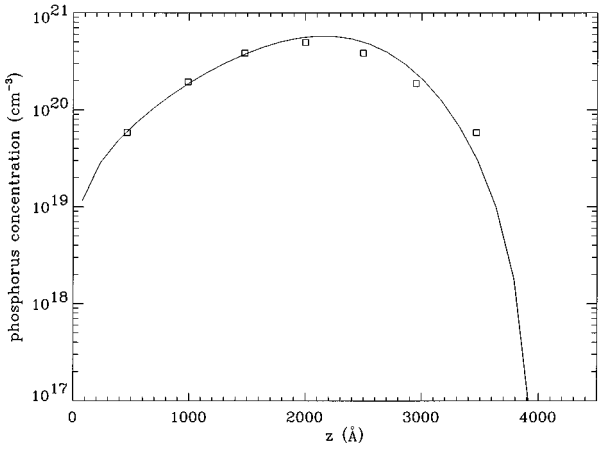

FIG. 6. Phosphorous-ion concentration for a 160-keV injected beam into amorphous silicon as a function of z: squares, experiment; line, TM.

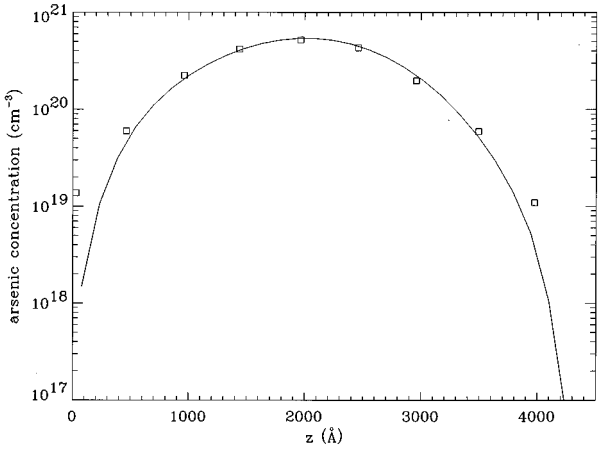

FIG. 7. Arsenic-ion concentration for a 355-keV injected beam into amorphous silicon as a function of z: squares, experiment; line, TM.

channel; otherwise excessive channeling can occur due to the finite size of the angular mesh.

Figure 8(a) shows the depth profile for the boron-ion concentration. Experimental results and results of an amorphous calculation and a channeling calculation are shown. It is obvious that channeled ions contribute to the tail of the concentration after the peak in the depth profile. Figures 8(b)–8(d) are the corresponding contour plots. The inclusion of channels allows the ions to penetrate further into the solid in preferred directions.

The computational requirements of the TM method depend strongly on the size of the mesh used and, to a lesser extent, the amount of large-angle scattering. For the results presented here, typical CPU time on a dedicated Hewlett-Packard 715/80 workstation is about 1 h (half of that if the symmetries of the model problems presented here were utilized). An equivalent computation using Monte Carlo (MC) methods [3] is reported to take 25–100 h.

Before concluding, a few remarks will be made about the similarities and differences between the TM method and existing techniques. While Boltzmann transport techniques are typically efficient, the implentation of these methods (e.g., Ref. [4]) in three dimensions would lead to unacceptable numerical diffusion during the process in which the ions' trajectories are integrated in space. The TM method overcomes this problem because it allows the ions to proceed from one nuclear scatter to the next directly. In this way, the TM method is more similar to MC methods. The key advantage to the TM method over the MC method is that instead of following discrete particles, the TM follows, in essence, a

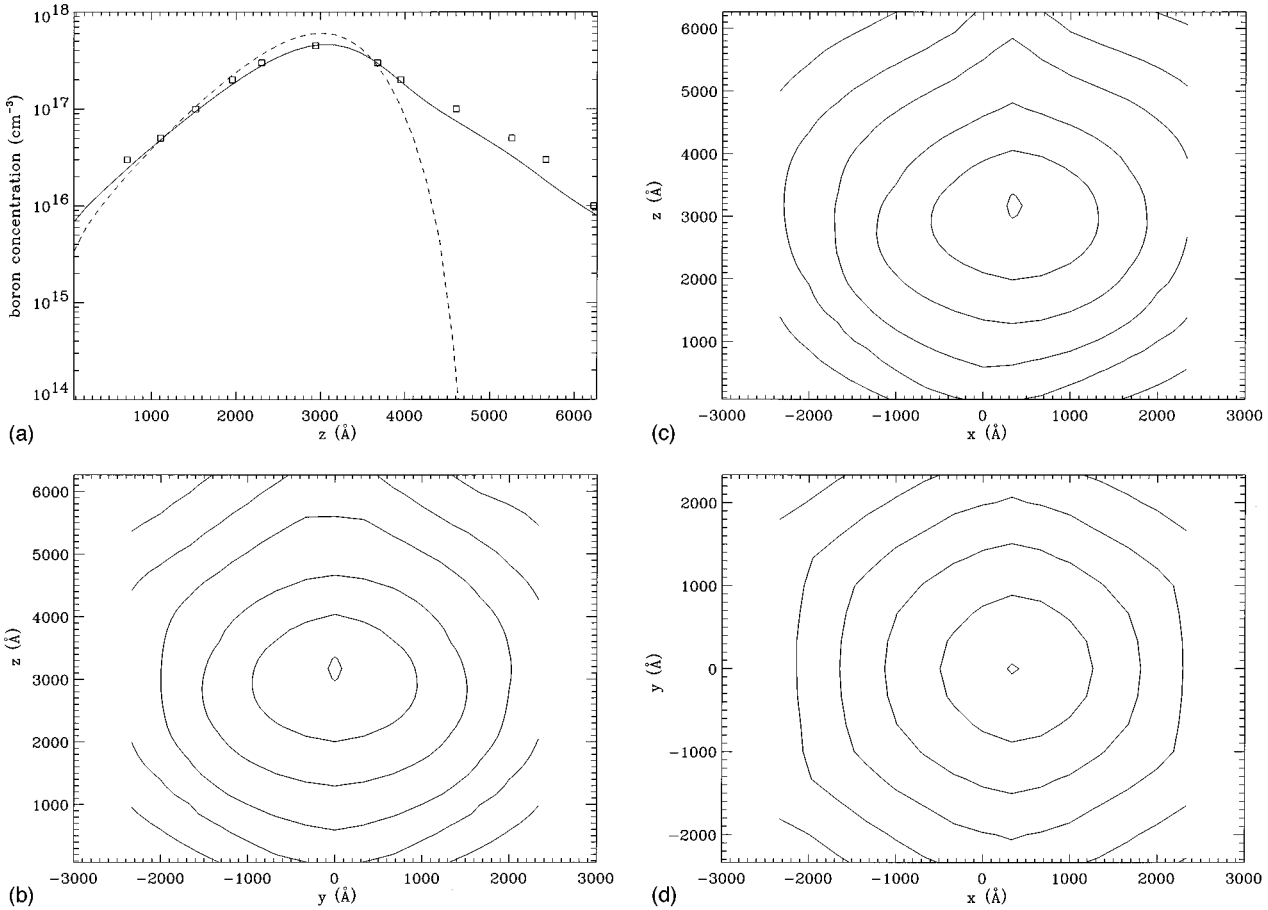

FIG. 8. Boron-ion concentration for an 85-keV injected beam into ⟨111⟩ silicon. (a) Boron-ion concentration as a function of z: squares, experiment; dashed line, amorphous TM calculation; solid line, channeling TM calculation. (b)–(d) Contour plots of the boron-ion concentration as a function of two spatial variables with the third being integrated (summed) over. Contours are 0.003 16, 0.01, 0.0316, 0.1, 0.316, and 0.95 of the maximum value.

density of ions. Therefore all possible trajectories (weighted by their corresponding probabilities) are incorporated into the TM, thereby eliminating statistical fluctuations.

In summary, we have presented a method of modeling ion implantation based on long-mean-free-path particle kinetics, which is highly efficient, accurate, and uses compact matrices to store the ''propagator'' needed for the calculation. Since the method only requires storage of scattering rates and the relatively simple angular distributions of scattered particles in each cell, rather than the full distribution function, one can use it to run a very large and detailed simulation on a relatively small computer. However, it is possible to derive the same information from this approach as one would with a full blown solution of the Boltzmann equation.

ACKNOWLEDGMENT

This work was supported in part by the National Science Foundation, Grant No. ECD-8721545.

[1] J. P. Biersack and L. G. Haggmark, Nucl. Instrum. Methods **174**, 257 (1980).

[2] J. Albers, IEEE Trans. Electron Devices **32**, 1930 (1985); J. Albers, *Results of the Monte Carlo Calculation of One- and Two-dimensional Distributions of Particles and Damage: Ion Implanted Dopants in Silicon*, Natl. Bur. Stand. (U.S.) Monograph 400-79 (U.S. GPO, Washingtion, DC, 1987).

[3] W. Bohmay, A. Burenkov, J. Lorenz, H. Ryssel, and S. Selberherr, IEEE Trans. Semicond. Manuf. **8**, 402 (1995).

[4] L. A. Christel, J. F. Gibbons, and S. Mylroie, J. Appl. Phys. **51**, 6176 (1980); M. D. Giles and J. F. Gibbons, IEEE Trans. Electron. Dev. **32**, 1918 (1985).

[5] J. F. Ziegler, U. Littmark, and J. P. Biersack, *The Stopping and Range of Ions in Solids* (Pergamon, Oxford, 1985), Vol. 1.

[6] R. E. P. Harvey, W. N. G. Hitchon, and G. J. Parker, J. Appl. Phys. **75**, 1940 (1994).

[7] R. E. P. Harvey, W. N. G. Hitchon, and G. J. Parker, IEEE Trans. Plasma Sci. **23**, 436 (1995).

[8] G. J. Parker, W. N. G. Hitchon, and D. J. Koch, Phys. Rev. E **51**, 3694 (1995).

[9] J. Lindhard, V. Nielsen, M. Scharff, and K. Dan Vidensk, Selsk. Mat. Fys. Medd. **36**, No. 10 (1968).

[10] O. B. Firsov, Zh. Eksp. Teor. Fiz. **32**, 1464 (1957); **34**, 447 (1958); **36**, 1517 (1959).

[11] F. H. Eisen, Can. J. Phys. **46**, 561 (1968).